Accurate and Robust Registration of Low Overlapping Point Clouds

Jieyin Yang[a,b], Mingyang Zhao[c,d], Xiaohong Jia[a,b], and Dong-Ming Yan[b,d]

[a]KLMM, Academy of Mathematics and Systems Science, Chinese Academy of Sciences, China
[b]University of Chinese Academy of Sciences, Beijing, China
[c]Beijing Academy of Artificial Intelligence
[d]State Key Laboratory of Multimodal Artificial Intelligence Systems (MAIS) & NLPR, Institute of Automation, Chinese Academy of Sciences

Abstract

Point cloud registration is fundamental to many computer graphics and visual tasks. Previous pairwise approaches mainly deal with the registration with a high overlapping hypothesis, while few existing methods explore the registration between low overlapping point clouds. However, the latter registration task is challenging and essential, since the weak correspondence in point clouds usually makes the algorithm tend to get stuck in a local minimum. In this paper, we present an accurate algorithm for the robust registration of low overlapping point clouds using optimal transformation. The core of our method is the effective integration of *geometric features* with the probabilistic model *hidden Markov random field*. First, we determine and remove the outliers of the point clouds by modeling a hidden Markov random field based on a high dimensional feature distribution. Then, we derive a *necessary and sufficient condition* when the symmetric function is minimized and present a new curvature-aware symmetric function to make the point correspondence more discriminative. Finally, we integrate our curvature-aware symmetric function into a geometrically stable sampling framework, which effectively constrains unstable transformations. We verify the accuracy and robustness of our method on a wide variety of datasets, particularly on low overlapping range scanned point clouds. Results demonstrate that our proposed method attains better performance with higher accuracy and robustness compared to representative state-of-the-art approaches.

Keywords:* *Point Cloud Registration, HMRF, Low Overlapping, Outliers, Probabilistic Model.

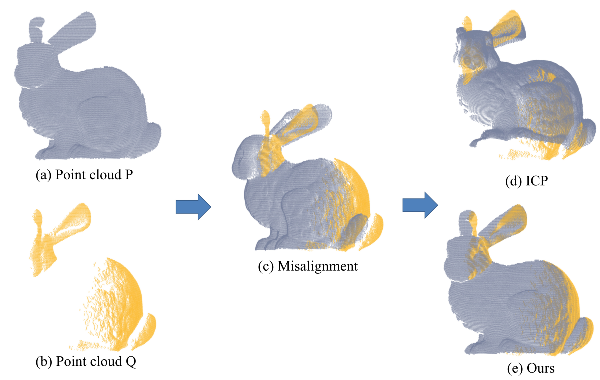

Figure 1. Low overlapping point cloud registration. ICP tends to get stuck into a local minimal due to insufficient correspondence, whereas our proposed method returns highly accurate registration.

1. Introduction

Point cloud registration is an important and fundamental task in computer graphics, computer vision, and robotics, which can be utilized for various applications, such as 3D scene reconstruction [11], simultaneous localization and mapping (SLAM) [26, 15], indoor scene modeling and cultural heritage management [36, 16], and so on. Given two partial range scans, our goal is to seek a *spatial transformation* comprising a 3D rotation matrix $\mathbf{R} \in SO(3)$[1] and a translation vector $\mathbf{t} \in \mathbb{R}^3$ to optimally align them into a common reference system.

The seminal work *iterative closet point* (ICP) [6] has become the most frequently used method for point cloud registration. It iteratively builds up the point proximity and calculates the transformation parameters via such as the *singular value decomposition* (SVD) [37]. However, there still exist several challenges in the development of a versatile or robust ICP. The primary challenge is the accurate registration of low overlapping point clouds caused by large per-

[1] $SO(3) := \{\mathbf{R} \in \mathbb{R}^{3\times 3} | \mathbf{R}\mathbf{R}^T = \mathbf{R}^T\mathbf{R} = \mathbf{I}_3, \det \mathbf{R} = 1\}$.

spective variations. As ICP highly depends on the initialization or correspondence, low overlapping inputs usually make it converge to a local minimum, as shown in Fig. 1. Although there are many variants of ICP existing in the literature, most of them target on robustness or efficiency. There still needs endeavor to explore and tackle this challenging low overlapping problem.

Recently, the *hidden Markov random field model* (HMRF) [9] is customized for point cloud registration problem [32], which shows potential power for dealing with low overlapping scans. However, it merely minimizes the point-to-point distance and ignores the 3D geometric features of point clouds, which empirically enables higher accuracy and more stable performance.

To explore geometric features and how to involve geometry into the probabilistic framework, in this work, we propose a new method for low overlapping point cloud registration, which attains better results in both accuracy and robustness. An overview of our method is shown in Fig. 2. Instead of using the distance as the single criterion when modeling HMRF, we also take geometric features such as the planarity and anisotropy into consideration. This gives a high dimensional feature distribution. Compared with distance residual, these features are more discriminative and effective, which help estimate the overlapping region more precisely, as shown in Fig. 2(b). In terms of the metric function, we utilize the symmetric distance including normals and curvatures for error measurement. We demonstrate that the proposed curvature-aware symmetric function results in more meaningful and distinguished punishment than [30]. Additionally, we point out that the classical point-to-plane metric [10] is a special case of our newly defined objective function around the plane point, *i.e.*, the point whose neighboring local surface is a plane. Based on this curvature-aware metric, we further use linear approximation of the objective function and incorporate it into a geometrically stable sampling framework, as presented in Fig. 2(c), in which we leverage the *matrix condition number* to achieve more stable transformations. Fig. 2(d) shows the intermediate result of our method after five iterations and the final registration result is shown in Fig. 2(e).

We conduct extensive experiments to validate the performance of the proposed method and compare it with representative state-of-the-art approaches on a wide variety of benchmark datasets. Results demonstrate that our method attains several salient advantages than competitors, *i.e.*, more accurate for low overlapping point clouds, as well as more robust against noise and outliers. To summarize, the main contributions of this work are as follows:

- We propose a novel method toward low overlapping point cloud registration via the effective integration of geometric features and probabilistic model HMRF, which achieves superior performance in both accuracy and robustness than competitors.
- We theoretically deduce the optimal condition of the symmetric function and incorporate curvature into it to make the optimization more discriminative.
- We introduce a geometry-aware point pair sampling process to improve the transformation stability.

2. Related Work

Due to the importance of point cloud registration on practical applications, extensive pioneer works have been made over the past several decades. The readers can refer to [35, 7] for more comprehensive study. Here, we put our focus on the rigid pairwise registration.

ICP-based Methods ICP proposed by [6] is one of the most famous point cloud registration algorithm. After its introduction, a lot of efforts have been devoted to improve its efficiency and robustness. The most popular modification for efficiency improvement is to refine the objective function of the original point-to-point distance by the point-to-plane manner [10], in which the l_2 distance from source points to the tangent planes of their corresponding points were calculated. Wang *et al.* [38] estimated the local surface around each point as a quadratic surface and introduced a squared distance function, which was then demonstrated theoretically and experimentally to have higher stability than the point-to-plane ICP [28]. Recently, Rusinkiewicz [30] raised a symmetric objective function taking normals of the point pairs into consideration, achieving the same simplicity and computational efficiency as the point-to-plane metric, yet with a wider convergence basin.

Besides the improvement of convergence speed, many work focused on the robustness promotion against noise and outliers. Among these algorithms, a popular attempt is to use robust estimators. Hontani *et al.* [20] revised the original l_2 norm of ICP as l_1 norm to increase the algorithm's sparsity and robustness. Moreover, sparse ICP [8] had their objective function based on the l_p norm with $p \in (0, 1)$ and optimized it by the iterative framework *Alternating Direction Method of Multipliers* (ADMM). Another line of work invoke *M-estimators* to depress the influence of large residuals. For example, fast global registration [41] took the Geman-McClure estimator as the penalty function and conducted the alignment in one single stage without the closest point queries, whereas Zhang *et al.* [40] utilized the Welsch function to enhance the robustness. Although these work are capable of relieving the outlier influence, when facing partially overlapping scenarios, they directly regard the points in non overlapping regions as outliers, hence are prone to misalignment. Several work had made attempts on low overlapping situations. For instance,

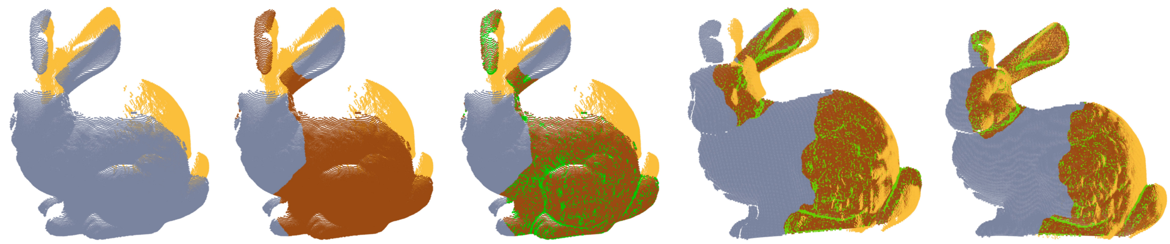

(a) Input (b) Inlier selection (c) Geometric constraint (d) Result after 5 iterations (e) Final result

Figure 2. Overview of the proposed framework: (a) Input point clouds. The blue and yellow models represent the source $\mathcal{P}$ and the target $\mathcal{Q}$, respectively. (b) Overlapping region estimation. Brown points represent inliers located in the overlapping region. (c) Construction of the geometric constraint with respect to inliers. Green points are selected under the curvature constraint and the point-pair sampling strategy. (d) The intermediate registration result after five iterations. (e) The final registration result when iterations converge.

[17] discarded point pairs whose distances surpass a certain threshold. Based on the neighbor priors, [32] distinguished the inliers in overlapping regions from outliers by modeling a hidden Markov random field, which showed advantages on moderate overlapping.

Statistics-based Methods Apart from the variants of ICP, statistical models are also customized for point cloud registration such as the *Gaussian Mixture Models* (GMM). Jian *et al.* [21] treated the source and the target point clouds as two GMMs, then the alignment problem was transformed into minimizing the discrepancy of the two probabilistic distributions under the KL divergence, while Tabib *et al.* [34] directly minimized the l_2 distance. Instead, coherent point drift (CPD) [27] described one of the point clouds as GMM, while the second set was realized via the *maximum likelihood estimation*. To encode more information into the statistical framework, Danelljan *et al.* [14] combined color feature with CPD together and designed the color-guided probabilistic registration method. Nevertheless, this algorithm is limited to the colorful point cloud registration task. To improve the robustness of statistical methods against the point density variation, Lawin *et al.* [23] modeled the underlying structure of the scene as a potential probability distribution and put forward a density adaptive point set registration method. In order to guarantee the convergence of CPD algorithm and overcome the shortcoming that CPD was relatively sensitive to rotation, [19] formulated coherent point drift in a Bayesian setting and leveraged variational inference for the transformation solving. Since statistical methods is based on the soft correspondence with probability, they are intrinsically robust. However, compared with ICP, these approaches usually have higher computational complexity.

Learning-based Methods With the advances of deep learning in recent years, people have tried applying neural networks for 3D point cloud registration. The typical idea is to replace main steps of the traditional pipeline in point cloud registration with learning-based modules. To be specific, Aoki *et al.* [5] combined PointNet [29] with Lucas-Kanade (LK) algorithm [25] into a trainable deep neural network named PointNetLK. Wang *et al.* [39] implemented ICP algorithm from a deep learning perspective, provided a simple structure to predict the relative position of two point clouds, and relieved the local optima problem in the classical ICP pipeline. Lu *et al.* [24] presented an end-to-end point cloud registration framework, in which the learned matching probability was used to generate corresponding points rather than selecting them from existing point pairs. Choy *et al.* [12] developed a differentiable framework for registration which contained three modules. Learning-based methods are able to represent features more effectively, nevertheless, they usually require longstanding training. As far as we know, the application of trained networks to point clouds out of the train or test set is not immediate, which is still an open problem.

3. Methodology

Given two point sets $\mathcal{P} = \{\mathbf{p}_i \in \mathbb{R}^3 \mid i = 1, 2, \cdots, n\}$ and $\mathcal{Q} = \{\mathbf{q}_j \in \mathbb{R}^3 \mid j = 1, 2, \cdots, m\}$ potentially scanned on the same object under different views, point cloud registration aims to find the optimal rigid transformation $(\mathbf{R}, \mathbf{t}) \in SO(3) \times \mathbb{R}^3$ to align the source point cloud $\mathcal{P}$ with the target one $\mathcal{Q}$. We first explore geometric features and how to integrate them with the hidden Markov model to make the pairwise correspondence more reliable.

3.1. Construction of Geometric Features

We adopt the *3D structure tensor* or 3D covariance matrix to describe the local geometric features of each point $\mathbf{p}_i \in \mathbb{R}^3$. The mean vector $\mu_i \in \mathbb{R}^3$ of the points in the neighborhood $\mathcal{N}_i$ of $\mathbf{p}_i$ is

$$\mu_i = \frac{1}{|\mathcal{N}_i|} \sum_{\mathbf{p}_k \in \mathcal{N}_i} \mathbf{p}_k, \tag{1}$$

where $\mathcal{N}_i = \{\mathbf{p}_k \in \mathbb{R}^3 | \|\mathbf{p}_k - \mathbf{p}_i\|_2 < r\}$ and $r > 0$ is the support radius. The covariance $\mathbf{\Sigma}_i$ is

$$\mathbf{\Sigma}_i = \frac{1}{|\mathcal{N}_i|} \sum_{\mathbf{p}_j \in \mathcal{N}_i} (\mathbf{p}_i - \mu_i)^T (\mathbf{p}_i - \mu_i). \tag{2}$$

Since $\mathbf{\Sigma}_i$ is symmetric and positive definite, we attain $\lambda_1 \geq \lambda_2 \geq \lambda_3 > 0$ after eigenvalue decomposition. We leverage the arithmetic combinations of eigenvalues to describe the local geometric features of each point. The planarity $\mathcal{P}$, anisotropy $\mathcal{A}$ and curvature $\mathcal{C}$ of $\mathbf{p}_i$ is adopted to accommodate our purpose:

$$\mathcal{P}_{p_i} = \frac{\lambda_2 - \lambda_3}{\lambda_1} \quad \mathcal{A}_{p_i} = \frac{\lambda_1 - \lambda_3}{\lambda_1} \quad \mathcal{C}_{p_i} = \frac{\lambda_3}{\lambda_1 + \lambda_2 + \lambda_3}. \tag{3}$$

3.2. Overlapping Region Estimation

To distinguish inliers in overlapping regions from outliers, similar to [32], we construct a probabilistic model based on the HMRF. We use $\mathbf{z}$ and $\mathbf{y}$ to represent the hidden field of the unobserved inlier or outlier state and the observed variables, respectively. In the work of [32], they directly choose the distance residual between the closest points as the observed variable $\mathbf{y}$, which possibly leads to misalignment when the initialization is unsatisfying. Fig. 3 shows the iterative process when applying the distance-based HMRF for registration. As is observed, it performs well under good initialization with the small rotation angle ($\rho = 15°$); however, as the rotation angle increases ($\rho = 30°$), indicating lower overlapping at initialization, the registration result starts to fail.

Different from the previous approach, in this work, we incorporate geometric features to the observed variable $\mathbf{y}$ and model the hidden Markov random field under high-dimensional probabilistic distributions. We define the observed variable $\mathbf{y} = [\mathbf{y}_1, \mathbf{y}_2, \mathbf{y}_3, \mathbf{y}_4]^T \in \mathbb{R}^4$, where $\mathbf{y}_1, \mathbf{y}_2, \mathbf{y}_3, \mathbf{y}_4$ denote the distance, the difference of planarity, anisotropy and curvature between closest points.

Given the observed variables $\mathbf{y}$, our target is to distinguish the inliers, namely the points in the overlapping region, from the outliers (the non overlapping points). The prior hypotheses we made are:

- The inliers typically lie closer to their closest points than the outliers.
- The geometry differences between inliers and their closest points are typically smaller than the outliers.
- The neighbors of the inlier tend to be inliers, while the neighbors of the outlier tend to be outliers.

According to these hypotheses, we adopt two normal distributions of different parameters *i.e.*, *normally distributed for inliers* and *normally distributed for outliers* to model $\mathbf{y}$. Since unobserved states $\mathbf{z}$ are modeled as a Markov random field, the probability distribution of $\mathbf{z}$ is a Gibbs distribution according to the Hammersley-Clifford theorem [13], *i.e.*,

$$P_G(\mathbf{z}) = W^{-1} \exp(-H(\mathbf{z})), \tag{4}$$

where $W = \sum_{\mathbf{z}} \exp(-H(\mathbf{z}))$ is the normalizing factor and $H(\mathbf{z})$ is the energy function. In our case, we choose the following energy function:

$$H(\mathbf{z}) = -\beta \sum_{i' \sim i} w_{i,i'} z_i z_{i'}, \tag{5}$$

where $w_{i,i'}$ represents the edge weight between z_i and $z_{i'}$ and $\beta \geq 0$ is a parameter relevant to the interactive strength. To simplify computation, we further use the mean field to approximate the posterior distribution $P_G(\mathbf{z}|\beta)$. Then the k-dimensional normal distributions are used to present the conditional density f. The detailed approximation steps and the final likelihood of the joint distribution are reported in *Supplemental Material*.

We adopt the *expectation maximization* (EM) algorithm to estimate the maximum likelihood parameters of the model and the hidden state. In E-step, we calculate the hidden state or posterior probability of the point cloud given the parameters, while in M-step, we calculate the parameters that maximize the expected likelihood. We present the theoretical deduction of the concrete EM steps in *Supplemental Material* for easy understanding. After the hidden state estimation, we choose the points $\mathbf{p}_i$ whose hidden state $z_i > 0$ and curvature $\mathcal{C}_{p_i} > \tau$ as inliers. Then we optimize the objective function defined in the following section.

3.3. Objective Function

The traditional point-to-plane ICP merely takes one normal into the objective function, recently [30] proves the potential of the symmetric function for point cloud registration

$$(\mathbf{p} - \mathbf{q}) \cdot (\mathbf{n}_p + \mathbf{n}_q), \tag{6}$$

where $\mathbf{n}_\star$ is the normal of a point $\star$. The analysis of the relative position of $\mathbf{p}$ and $\mathbf{q}$ in Eq. 6 gives the following conclusion.

Proposition 1 *Points $\mathbf{p}$ and $\mathbf{q}$ and their normals $\mathbf{n}_p$ and $\mathbf{n}_q$ lie in the same cylinder, if and only if Eq. 6 equals to zero.*

Theoretic proof is presented in *Supplemental Material*. From the proof, we conclude that without the consideration of the geometric characteristics of each point, all cylinders with arbitrary circle radius satisfy the above condition, and the residual generated by their points get no punishment.However, we mainly want the point pairs with the same geometric characteristic (the local surfaces around

(a) Input (b) #interation=1 (c) #interation=5 (d) #interation=10 (e) Final result

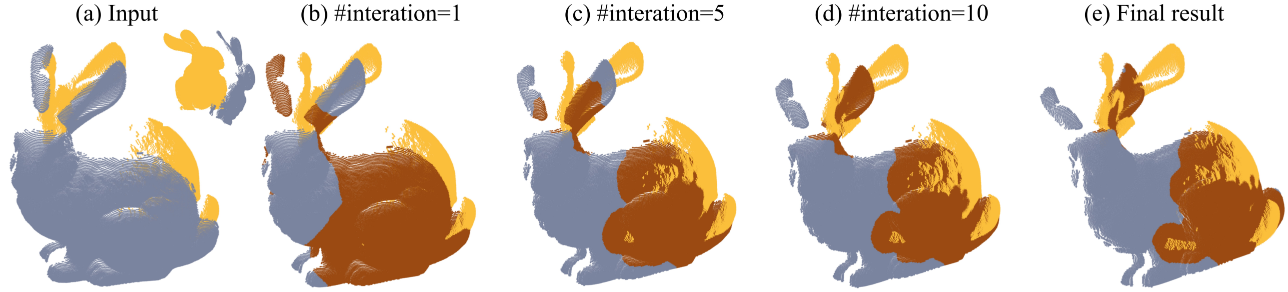

(a) Input (b) #interation=1 (c) #interation=3 (d) #interation=10 (e) Final result

Figure 3. The iterative process of [32] with the rotation angle $\rho = 15°$ (top) and $\rho = 30°$ (down), where brown region indicates the estimated overlapping part. As observed, [32] converges to a local minimal when the initialization is unsatisfying ($\rho = 30°$).

both points are the same) to slide between each other without punishment. To this end, we further consider the curvature feature, then the improved objective function is

$$(\mathbf{p}-\mathbf{q})\cdot(\bar{\mu}_q\mathbf{n}_p+\bar{\mu}_p\mathbf{n}_q), \tag{7}$$

where $\bar{\mu}_p = \mu_p/(\mu_p+\mu_q)$ and $\bar{\mu}_q = \mu_q/(\mu_p+\mu_q)$ are normalized curvatures of $\mathbf{p}$ and $\mathbf{q}$, respectively. From Eq. 7, we observe that when the curvature $\mu_p = \mu_q$, the objective function is equivalent to the primary symmetric objective function. However, when the curvature $\mu_p \gg \mu_q$, $\bar{\mu}_q \approx 0$, we can approximate the local surface around $\mathbf{q}$ as a plane. In this situation, our proposed objective function (Eq. 7) is equivalent to the popular point-to-plane function. Therefore, our objective function of the two point clouds $\mathcal{P}$ and $\mathcal{Q}$ is defined as

$$\sum_{i=1}^{n}\|(\mathbf{R}\mathbf{p}_i-\mathbf{R}^{-1}\mathbf{q}_i+\mathbf{t})\cdot(\bar{\mu}_{q,i}\mathbf{n}_{p,i}+\bar{\mu}_{p,i}\mathbf{n}_{q,i})\|_2^2. \tag{8}$$

3.4. Stable Point-Pair Sampling

After the determination of the overlapping region between two point clouds, we further propose a point-pair sampling strategy to constrain the uncertainty transformation based on the curvature aware symmetric function, by which the registration becomes more stable in the existence of large percentage of non-feature points. Like [30], we adopt linear approximation to transform Eq. 8 as

$$\sum_{i=1}^{n}\|((\tilde{\mathbf{p}}_i-\tilde{\mathbf{q}}_i)\cdot\mathbf{n}_i+((\tilde{\mathbf{p}}_i+\tilde{\mathbf{q}}_i)\times\mathbf{n}_i)\cdot\tilde{\mathbf{a}}+\mathbf{n}_i\cdot\tilde{\mathbf{t}})\|_2^2, \tag{9}$$

where $\bar{\mathbf{p}}$ and $\bar{\mathbf{q}}$ are the mean value of selected points $\mathbf{p}_i$ and its correspondence $\mathbf{q}_i$. We have $\tilde{\mathbf{p}}_i = \mathbf{p}_i - \bar{\mathbf{p}}$, $\tilde{\mathbf{q}}_i = \mathbf{q}_i - \bar{\mathbf{q}}$, $\mathbf{n}_i = \bar{\mu}_{q,i}\mathbf{n}_{p,i} + \bar{\mu}_{p,i}\mathbf{n}_{q,i}$. Considering the last two terms of Eq. 9, we figure out that the i^{th} term of the objective function will change if the given vector $[(\tilde{\mathbf{p}}_i+\tilde{\mathbf{q}}_i)\times\mathbf{n}_i, \mathbf{n}_i]$ is moved by the transformation vector $[\Delta\tilde{\mathbf{a}}^{\mathrm{T}}, \Delta\tilde{\mathbf{t}}^{\mathrm{T}}]$:

$$\Delta e_i = \left[\Delta\tilde{\mathbf{a}}^{\mathrm{T}}, \Delta\tilde{\mathbf{t}}^{\mathrm{T}}\right]\begin{bmatrix}(\tilde{\mathbf{p}}_i+\tilde{\mathbf{q}}_i)\times\mathbf{n}_i\\ \mathbf{n}_i\end{bmatrix}. \tag{10}$$

Eqs. 9 and 10 show that if the vector $[(\tilde{\mathbf{p}}_i+\tilde{\mathbf{q}}_i)\times\mathbf{n}_i, \mathbf{n}_i]$ is perpendicular to $[\tilde{\mathbf{a}}, \tilde{\mathbf{t}}]$, then the value of the objective function will not change. From the above analysis, we investigate the covariance matrix $\mathbf{C} \in \mathbb{R}^{6\times 6}$:

$$\mathbf{C} = \begin{bmatrix}(\tilde{\mathbf{p}}_1+\tilde{\mathbf{q}}_1)\times\mathbf{n}_1 & \cdots & (\tilde{\mathbf{p}}_n+\tilde{\mathbf{q}}_n)\times\mathbf{n}_n\\ \mathbf{n}_1 & \cdots & \mathbf{n}_n\end{bmatrix} \cdot \begin{bmatrix}((\tilde{\mathbf{p}}_1+\tilde{\mathbf{q}}_1)\times\mathbf{n}_1)^{\mathrm{T}} & \mathbf{n}_1^{\mathrm{T}}\\ \vdots & \vdots\\ ((\tilde{\mathbf{p}}_n+\tilde{\mathbf{q}}_n)\times\mathbf{n}_n)^{\mathrm{T}} & \mathbf{n}_n^{\mathrm{T}}\end{bmatrix}. \tag{11}$$

The matrix $\mathbf{C}$ encodes the error variations when the source point cloud $\mathcal{P}$ is moved from its ground-truth location (which is aligned with the target point cloud $\mathcal{Q}$) by transformation $[\Delta\tilde{\mathbf{a}}, \Delta\tilde{\mathbf{t}}]$:

$$\Delta\epsilon = \left[\Delta\tilde{\mathbf{a}}^{\mathrm{T}}, \Delta\tilde{\mathbf{t}}^{\mathrm{T}}\right]\ \mathbf{C}\ \begin{bmatrix}\Delta\tilde{\mathbf{a}}\\ \Delta\tilde{\mathbf{t}}\end{bmatrix}. \tag{12}$$

Suppose the ordered eigenvalues of $\mathbf{C}$ after eigenvalue decomposition are $\lambda_1 \geq \lambda_2 \geq \cdots \geq \lambda_6$ and their corresponding eigenvectors are $\mathbf{x}_1, \mathbf{x}_2, \cdots, \mathbf{x}_6$, we find that if the transformation parameters $[\Delta\tilde{\mathbf{a}}, \Delta\tilde{\mathbf{t}}]$ equal to the eigenvector whose corresponding eigenvalue is relatively small, then in this direction the changed error $\Delta\epsilon$ in Eq. 12 will also be small. As is defined in [18], we term this *unconstrained direction*. In order to avoid the possible unconstrained direction, we sample the point pairs to let the condition number $c = \frac{\lambda_1}{\lambda_6}$ of $\mathbf{C}$ as close to one as possible. See *Supplemental Material* for a detailed introduction to our geometry induced sampling method and the pseudo-code of our point-pair sampling process.

4. Experimental Evaluations and Discussion

In this section, we perform extensive experiments to evaluate the accuracy, robustness, and efficiency of the proposed method, and compare it with representative state-of-the-art approaches. The implementation of these competitors are publicly available online and their detailed parameter settings are listed in *Supplemental Material*. We adopt the following *root mean-squared error* (RMSE) to quantitatively measure the registration quality

$$\mathbf{RMSE} = \sqrt{\frac{1}{N}\sum_{i=1}^{N} \|\hat{\mathbf{R}}\mathbf{p}_i + \hat{\mathbf{t}} - \mathbf{R}_g\mathbf{p}_i - \mathbf{t}_g\|_2^2}, \quad (13)$$

where $(\hat{\mathbf{R}}, \hat{\mathbf{t}})$ and $(\mathbf{R}_g, \mathbf{t}_g)$ represent the estimated and the ground truth transformation, respectively. We use 10-nearest-neighborhood points for normal calculation. To be statistically representative, we perform 50 experiments for each test and report the average performance of the RMSE and timings. All experiments are executed on a laptop with a 2.50 GHz Intel Core i5-7200 and 4 GB RAM.

Accuracy Test Firstly, we use four point cloud datasets from the Stanford 3D Scanning Repository [3], *i.e.*, Bunny, Armadillo, Dragon, and Buddha for accuracy test. They are captured by a Cyberware 3030 MS laser scanner with different scanning perspectives, thereby having partial overlappings, as illustrated in the first column of Fig. 4. We compare the proposed method with the Point-to-Point ICP (P2P-ICP) [6], Point-to-Plane ICP (P2N-ICP) [10], HMRF-ICP [32], as well as two popular statistics-based registration methods including GMM [21] and CPD [27]. The statistical results of each compared method are reported in Table 1. From which, we conclude that the proposed method attains the overall highest accuracy, *i.e.*, the top accuracy on Bunny, Armadillo and Baddaha, and the second best accuracy on Dragon. P2P-ICP and P2N-ICP are efficient, but their RMSE are relatively larger than ours. HMRF-ICP consumes more overall time than ours, however, its registration accuracy is still unsatisfying, since its average RMSE are almost 10 times larger than ours. CPD achieves higher accuracy than GMM, especially on Armadillo and Baddaha, nevertheless, both of them are subject to highly computational complexity. We present several registration examples in Fig. 4, where the color maps in the lower right indicate the registration deviations under the logarithmic scale.

Robustness Against Noise Subsequently, we assess the robustness of the proposed method against noisy data. To this end, we add a series of Gaussian noise with zero mean and different variance to the source point cloud of the friends dataset [2]. The variance $\sigma^2 \in [0.00, 0.09]$ is varied with the step size equal to $\Delta\sigma^2 = 0.01$. We further compare our method with the robust approaches include Generalized ICP (G-ICP) [31], Fast Global Registration (FGR) [41], Sparse ICP (S-ICP) [8], Fast and Robust ICP (FR-ICP) [40]. The test results are reported in Fig. 5(a). As observed, the methods P2N-ICP, GMM and G-ICP, showing significant deviations, are more sensitive to noise than the rest ones. With noise level increasing, FGR starts producing large RMSE, indicating that it is less robust to heavy noise. In contrast, CPD, FR-ICP and Ours achieve the overall highest robustness, also, they are substantially stable. Fig. 6 exhibits the comparison samples of all compared methods under the contamination of $\sigma^2 = 0.06$.

Robustness Against Outliers We also test the influence of outliers for point cloud registration. We adopt the Bimba dataset from the AIM@SHAPE repository [2] for test. Some samples are illustrated in Figs. 7(a) and 7(b). Outliers are uniformly distributed within the bounding box of the source point cloud, and the number of them is equal to λN, where N is the amount of the original points, and $\lambda \in \{1\%, 3\%, 5\%, 10\%, 20\%, 50\%, 100\%, 200\%\}$. According to Fig. 5(b), we conclude that FR-ICP and our proposed method are more robust against outliers than competitors. HMRF-ICP has the third best performance, nevertheless, its time consumption is twice as much as ours. For the other ICP-based methods, they get significant deviations when outliers are over 20%, partially because of the poor initialization and the erroneous correspondence caused by outliers. Outliers have a degree of impacts on statistics-based methods, since they keep relatively stable performance, which can be attributed to their soft correspondence scheme with probability. However, they show low-quality registration results even without the existence of outliers, hence they are preferable to coarse registration tasks. Instead, our method exhibits highly accurate registration performance. Fig. 7(a) and 7(b) present several comparison samples with $\lambda = 50\%$ and 200%, respectively.

Initialization Impact Next, we evaluate the performance of all algorithms under different initialization. For this purpose, we exert various rotation angles to the source point cloud of the Berkeley Angel dataset [22], of which the main

Table 1. Quantitative results of average RMSE and computation time (in seconds) with different registration methods on Stanford datasets. **Bold** fonts indicate the best performance. Our method attains the overall best accuracy along with reasonable runtime.

Methods	Bunny		Armadillo		Dragon		Buddha	
	RMSE	Time	RMSE	Time	RMSE	Time	RMSE	Time
P2P-ICP [6]	0.145	**4.53**	0.076	0.80	0.057	0.80	0.078	3.35
P2N-ICP [10]	0.132	15.64	0.018	**0.53**	0.023	**1.17**	0.054	**1.74**
GMM [21]	0.286	73.42	0.154	50.39	0.057	56.76	0.217	15.06
CPD [27]	0.238	276.25	0.037	150.80	**0.013**	158.24	0.027	260.66
HMRF-ICP [32]	0.207	24.30	0.102	8.03	0.037	7.28	0.112	13.88
Ours	**0.027**	5.42	**0.017**	6.78	0.018	7.29	**0.019**	7.86

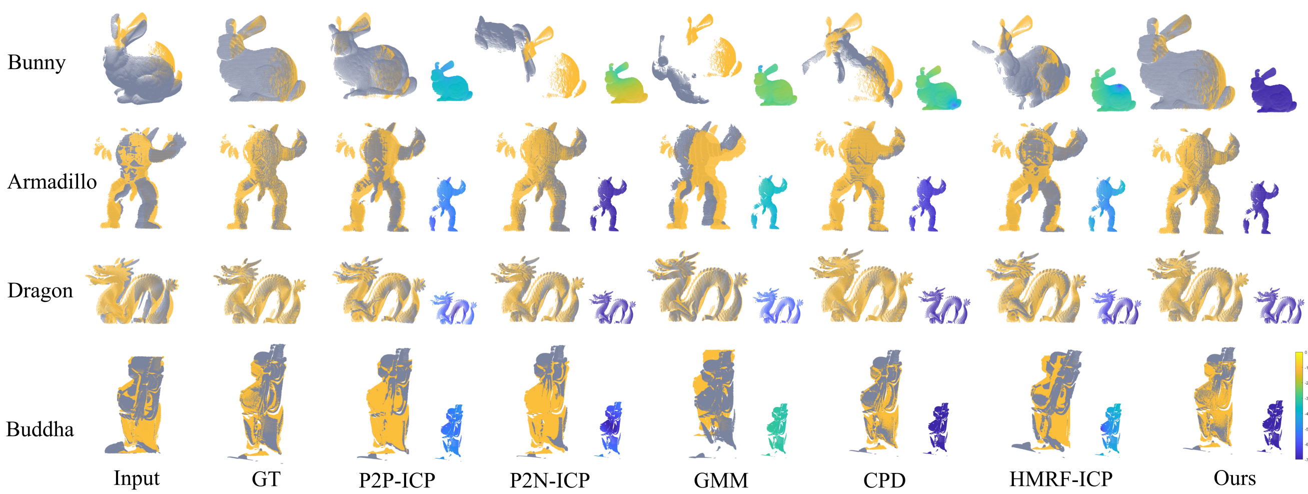

Figure 4. Registration results on four Stanford scanning datasets. The color-coding in bottom right visualizes the error between the registration results and the ground-truth alignments.

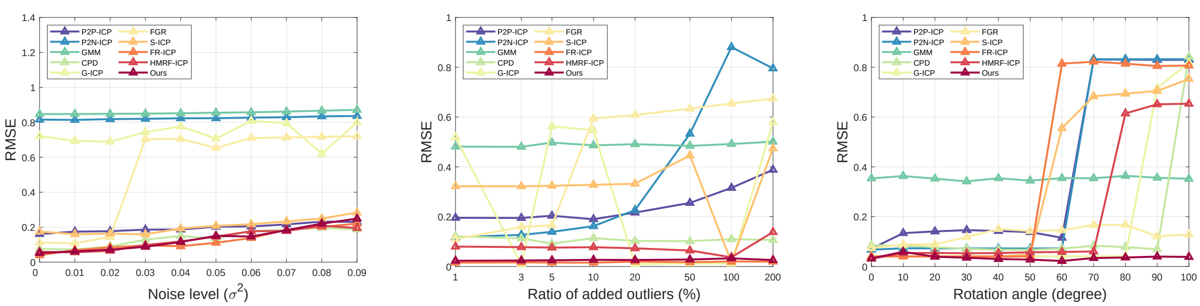

(a) RMSE with different noise (b) RMSE with different outliers (c) RMSE with different initial angles

Figure 5. Statistic of RMSE under different test settings. (a) RMSE with different noise levels, where noise variance σ^2 ranges from 0.00 to 0.09. (b) RMSE with different outlier ratios $\{1\%, 3\%, 5\%, 10\%, 20\%, 50\%, 100\%, 200\%\}$. (c) RMSE with different initial rotation angels, where θ ranges from 0° to 100°.

axis is attained by principle component analysis (PCA). The rotation angle ρ changes from 0° to 100° with the step size equal to 10°. Note that large rotation angles indeed indicate lower overlappings at initialization. We report the test results in Fig. 5(c), where we observe that except GMM, all methods perform well when $\rho \leq 50^\circ$. However, as rotation angles become larger, FR-ICP and S-ICP return significant errors. P2P-ICP and P2N-ICP share the similar performance, and their maximum angle tolerance or breakdown point is 60°. When $\rho > 70^\circ$, HMRF-ICP also generates large deviations, whereas our method works fairly well even under $\rho = 100^\circ$. Additionally, the proposed method is more stable than CPD and achieves the highest accuracy, where its RMSE is still less than 0.05 at $\rho = 100^\circ$. We present registration results with the misalignment angle $\rho = 90^\circ$ in Fig. 8.

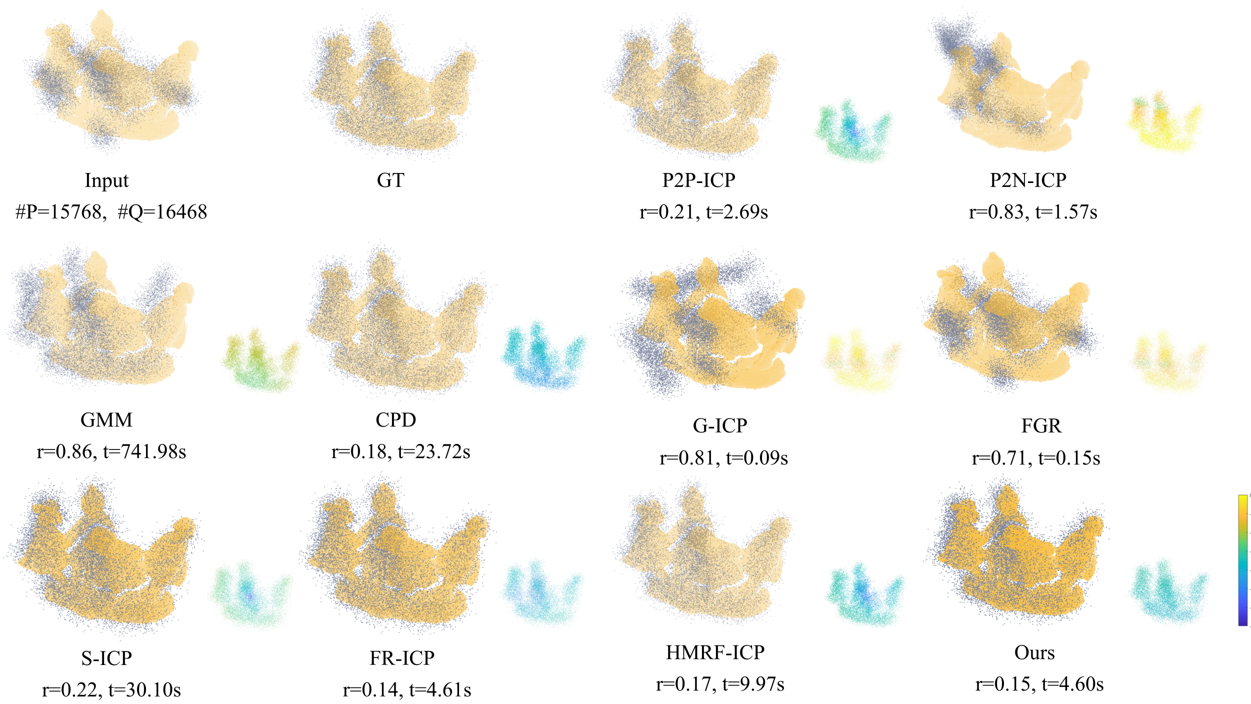

Figure 6. Comparison samples of different methods under noise contamination σ^2 =0.06. The blue and the yellow models represent the source and the target point clouds $\mathcal{P}$, $\mathcal{Q}$, respectively. #P and #Q denote their point number. RMSE (abbreviated as r) and the runtime (t) are reported under each result. The log-scale color map in bottom right visualizes the registration error compared with the ground-truth alignments. Our proposed method attains the second highest registration accuracy with comparable speed.

Low Overlapping Test Previous experiments have demonstrated the promising performance of the proposed method, in this test, we assess its performance with respect to the low overlapping point clouds specially. This case is difficult to handle yet frequently emerges in real-world scenarios. Apart from previous competitors, we further involve RANSAC optimized in Open3D library [2] for comparison. We use two range scans from the TUM RGB-D dataset [33] which have a low rate of overlapping, as illustrated in Fig. 9. The RMSE and runtime of each method are reported under their registration results in Fig. 9. Results demonstrate that traditional ICP-based methods (P2P-ICP and P2N-ICP) suffer from high RMSE in low overlapping situations, hence good initialization is usually required. The statistics based methods (GMM and CPD) get high RMSE since they also take outliers (points in the non-overlapping region) into consideration. Because of erroneous correspondence or false judgement of outliers, FR-ICP and S-ICP also generate high RMSE. Although G-ICP, FGR, RANSAC and HMRF-ICP have relatively lower RMSE compared to the aforementioned methods, their registration results are not accurate enough. However, our proposed method attains the lowest RMSE with comparable convergence speed. The reason is that based on the geometric features, it is able to select the right inliers from input points for registration, meanwhile reject the outliers in non-overlapping domains. Nevertheless, traditional ICP-based methods treat all points equally as inliers, hence are prone to resulting in deviations.

Furthermore, we design experiments to analyze the influence of different overlapping rates on registration results. We choose four representative methods in our experiments, namely Sparse ICP, Fast and Robust ICP, HMRF-ICP and Ours, since they are designed to be more robust to low overlapping cases. For comparison, we randomly select eight kinds of point clouds from the TUM RGB-D dataset [33], with their adjacent interval $\alpha \in \{1, 2, 3, 4, 5, 10, 15, 20\}$. For instance, when $\alpha = 5$, the target and source point clouds required registration have indexes $(0, 5), (1, 6), \cdots$. The overlapping rate will get much lower as α increases. For each class point cloud, we use 100 frames to ensure the overlapping rate changing from 5% to 100% for test, hence there are in total of 800 point cloud pairs for registration. The overlapping rate of each pair is estimated as follows:

$$\begin{aligned} d_1 &:= \mathrm{dist}(\mathbf{p}, \mathbf{p}_{\text{nearest}}) \\ d_2 &:= \mathrm{dist}(\mathbf{p}, \mathbf{q}_{\text{nearest}}) \end{aligned} \tag{14}$$

$$\chi_A(\mathbf{p}) = \begin{cases} 1 \quad if \quad \dfrac{d_2}{d_1} < \epsilon \\ 0 \quad otherwise \end{cases} \tag{15}$$

the source point $\mathbf{p}$ is considered to be on the overlapping region A if the distance d_2 to its nearest point of another

[2] https://github.com/isl-org/Open3D

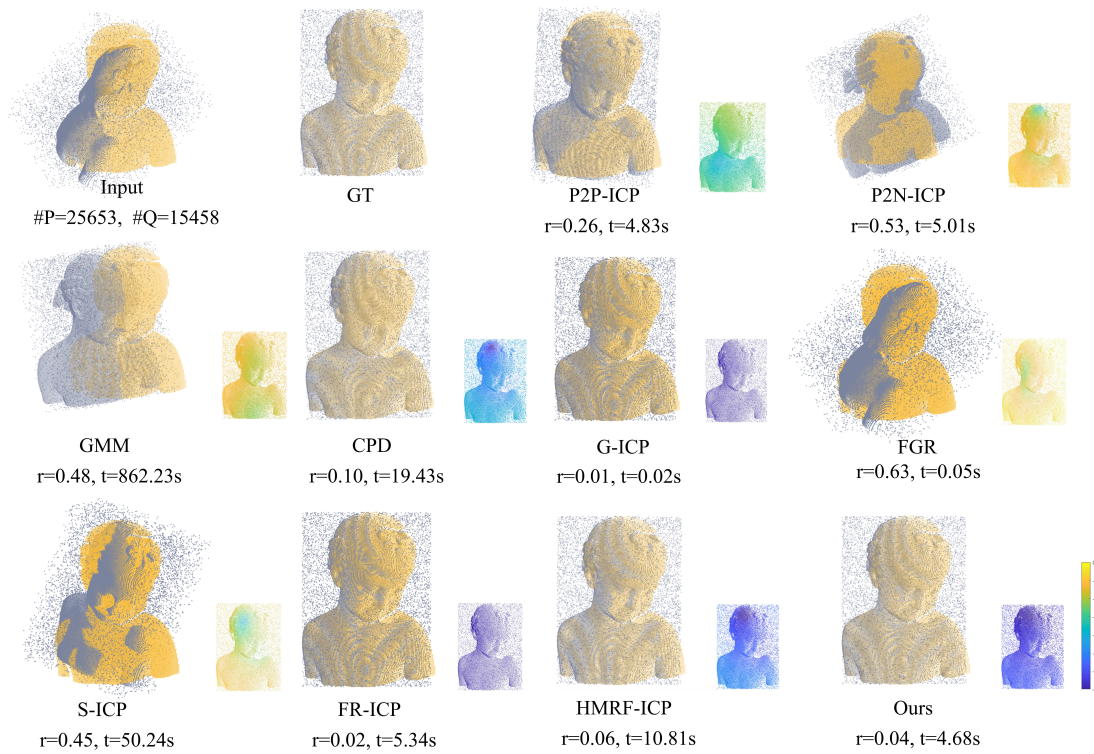

(a) Registration results under 50% outliers

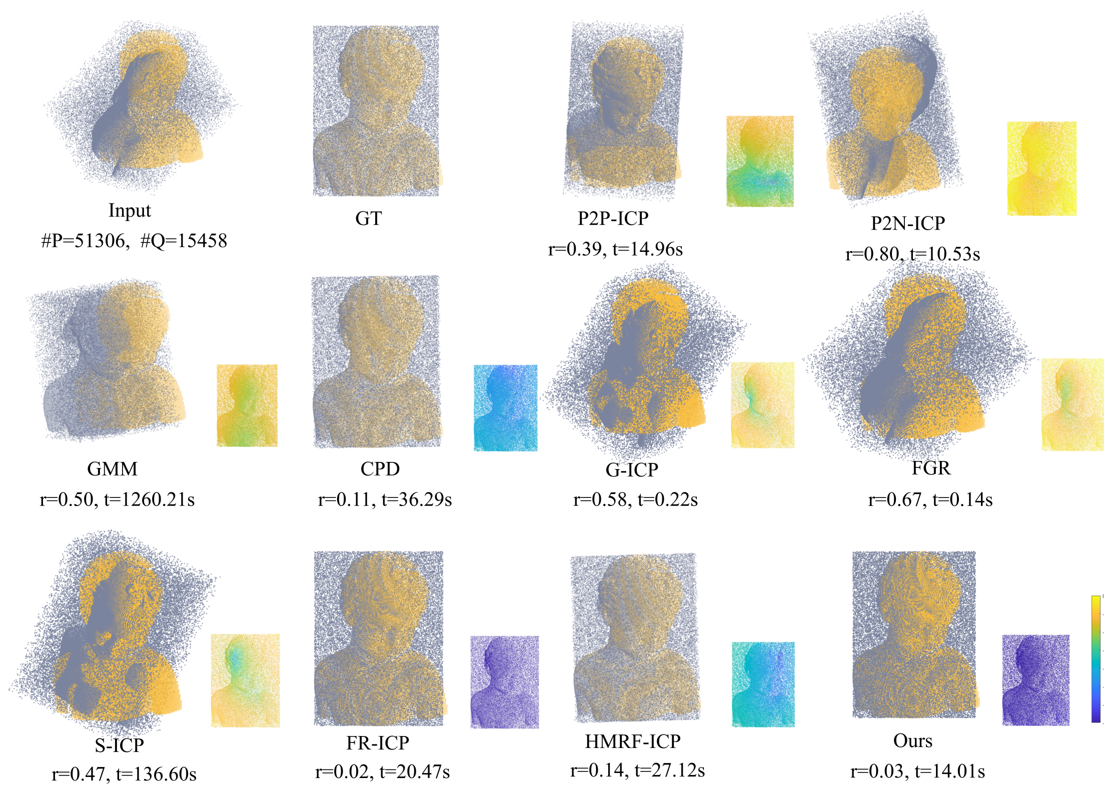

(b) Registration results under 200% outliers

Figure 7. Qualitative comparison under the contamination of (a) 50% and (b) 200% outliers. In situation of 50% outliers, G-ICP attains the highest accuracy with the least computation time, while our method also gets promising result. For 200% outliers, our method still successfully registers the point clouds, along with fairly lower RMSE and fast speed.

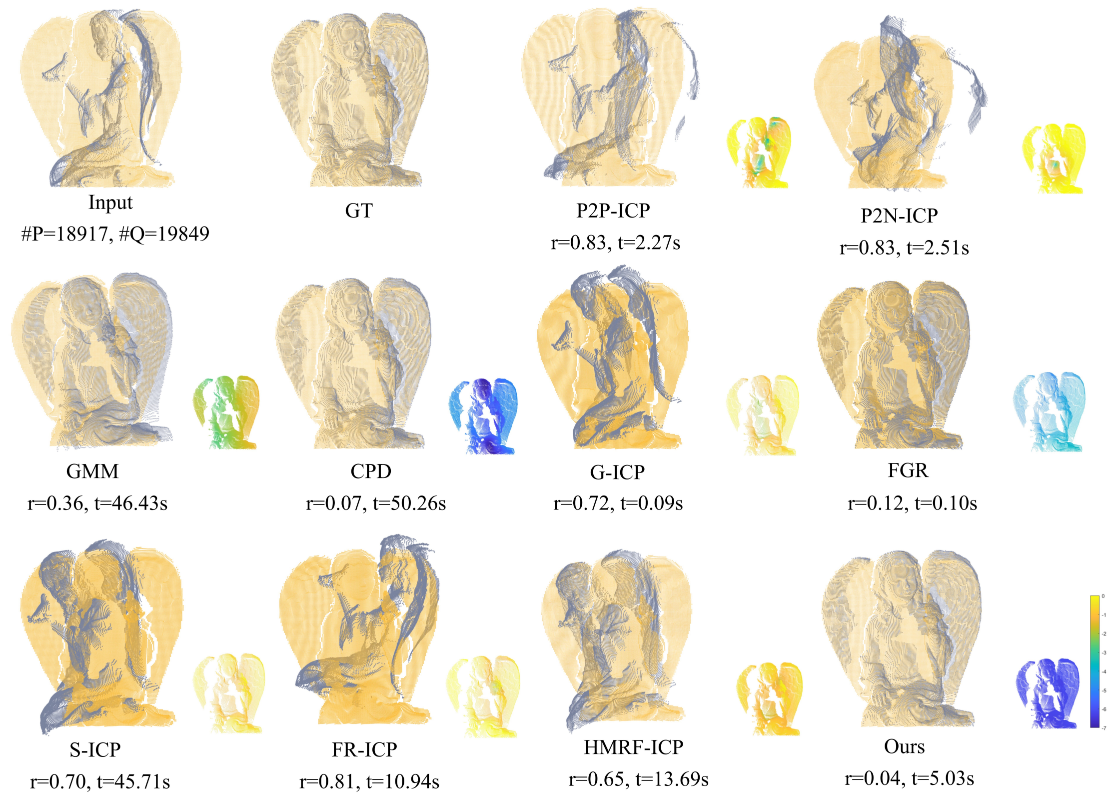

Figure 8. Comparison samples under the initial rotation angle $\rho = 90^{\circ}$. Our method outperforms the others with higher registration accuracy, especially under large initial rotation angles or low overlappings.

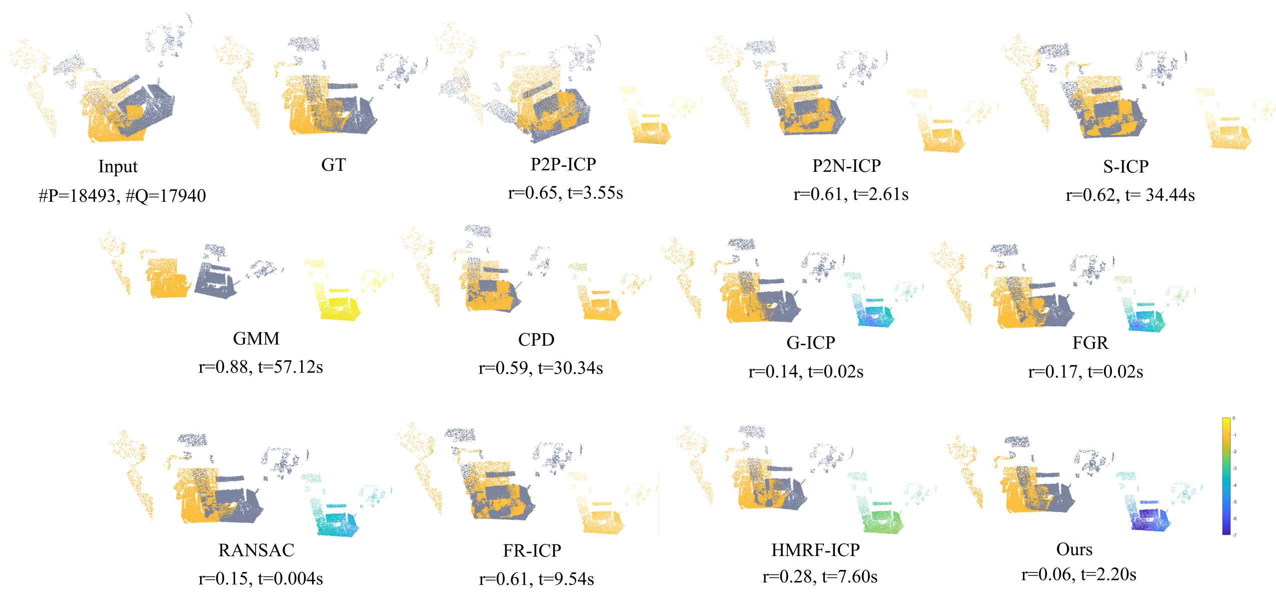

Figure 9. Registration results of different methods for the low overlapping model. Our method outperforms all competitors with the highest registration accuracy, meanwhile having a reasonable time consumption.

point cloud $\mathbf{q}_{nearest}$ versus the distance d_1 to the nearest point of its point cloud $\mathbf{p}_{nearest}$ in Eq. 14 is less than certain threshold. In our experiments, we set the default tolerance ϵ to be 15 in Eq. 15.

The three rows in Fig. 10 show the influence of different overlapping rates on RMSE, translation error and rotation error, respectively. We figure out that when the overlapping rate is high, all methods work well and FR-ICP has the min-

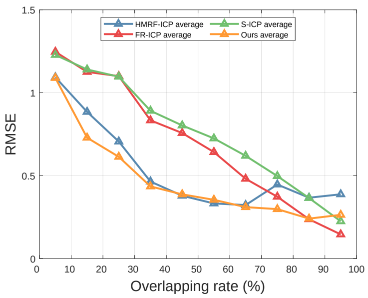

(a) Average RMSE

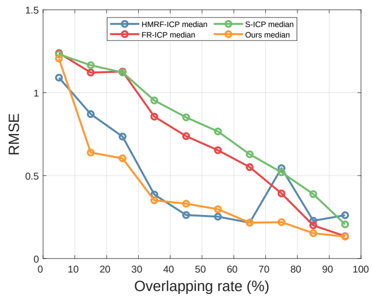

(b) Median RMSE

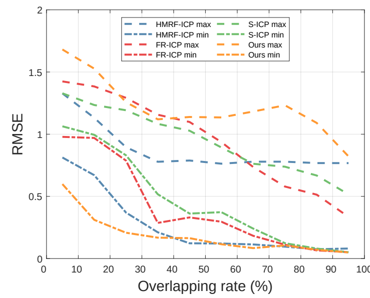

(c) Max and Min RMSE

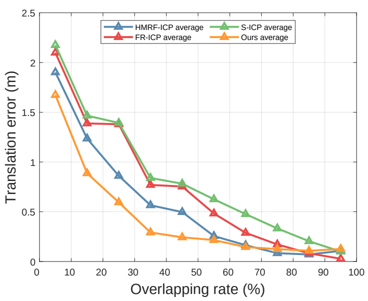

(d) Average translation error

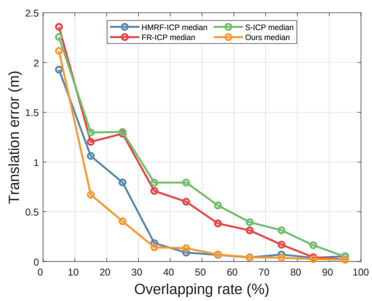

(e) Median translation error

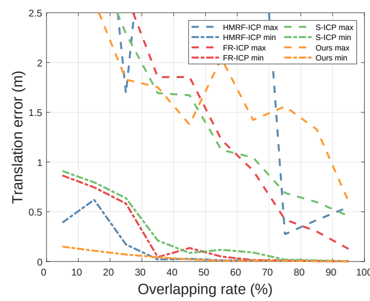

(f) Max and Min translation error

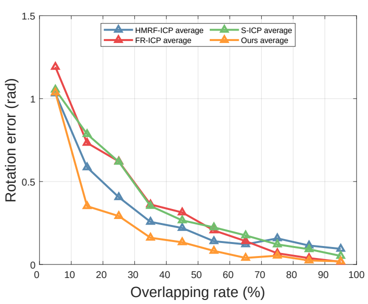

(g) Average rotation error

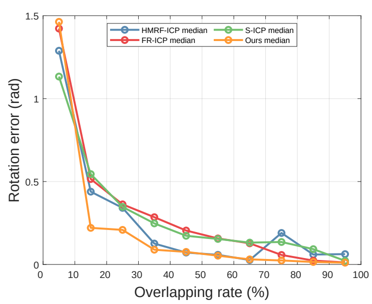

(h) Median rotation error

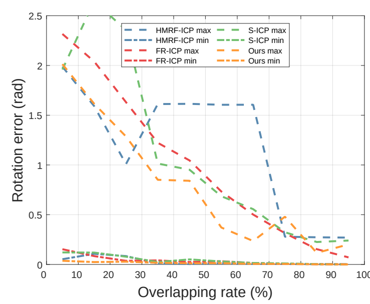

(i) Max and Min rotation error

Figure 10. Quantitative results of RMSE, translation error, and rotation error under a set of overlapping rates. We present the average, median, and maximum-minimum value on the first, second, and third column, respectively. As observed, the error increases when the overlapping rate decreases.

imum average RMSE. However, when the overlapping rate decreases, its performance deteriorates rapidly. Its median RMSE exceeds 0.5 when the overlapping rate is less than 70%. HMRF-ICP and our method perform well at moderate overlapping rate, and our method has lower translation error and rotation error in average. When overlapping rate is below 20%, no methods perform fairly well on all cases, but our method can still work well on some cases since the minimum RMSE, translation error and rotation error of our method are the lowest compared with the others. Therefore, we conclude that our method has wider convergence basin than competitors under low overlapping settings. We present a test sample with the low overlapping rate equal to 0.3999 in Fig. 11. More experimental results of different approaches under different overlapping rates are reported in *Supplemental Material*.

Sequence Point Cloud Test In this section, we evaluate the performance of each method on sequence point clouds. We adopt the ETH laser dataset[4] and the KITTI dataset[1] for test. For the ETH laser dataset, the ”Apartment” sequence that contains 45 point clouds are used. We align the adjacent point cloud pairs in the sequence and calculate the RMSE as well as the running time. Since the number of points is too large in raw data, we randomly sample 20% candidate points for registration. However, methods like CPD and GMM still suffer from fairly high computational complexity, hence the number of candidate points for these two methods is further reduced to seven thousand. From the result presented in Fig. 12, we observe that our method

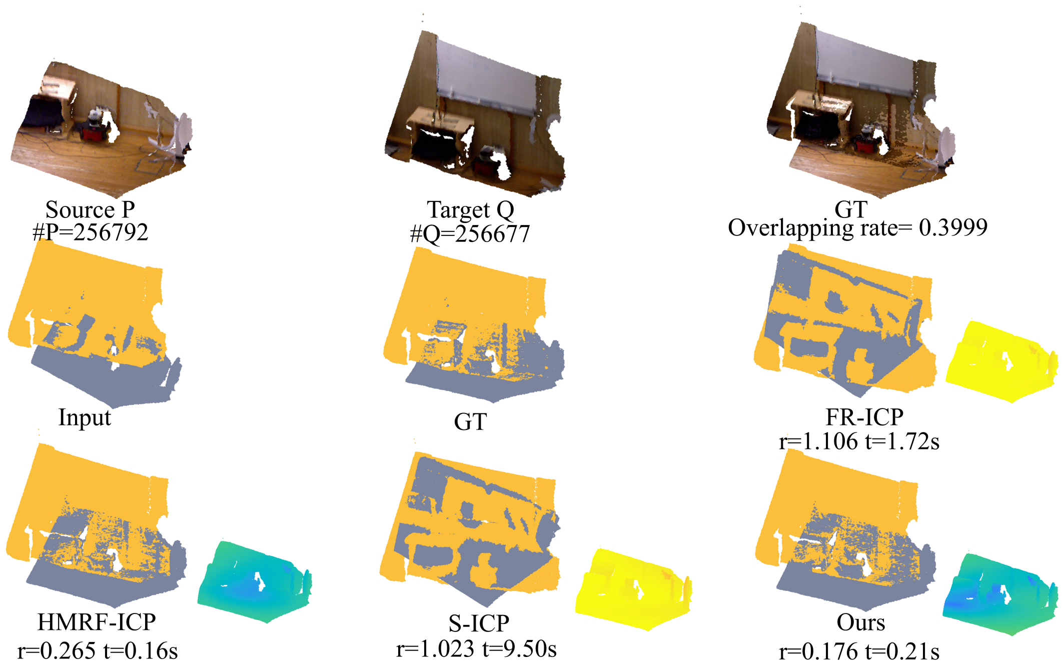

Figure 11. Registration results when overlapping rate equals to 0.3999. The first row illustrates the original point clouds attained based on RGB image and depth map. The second row and the third row show the registration results of different methods and their log-scale color coding. As observed, our proposed method achieves the most reliable registration under low overlapping rate.

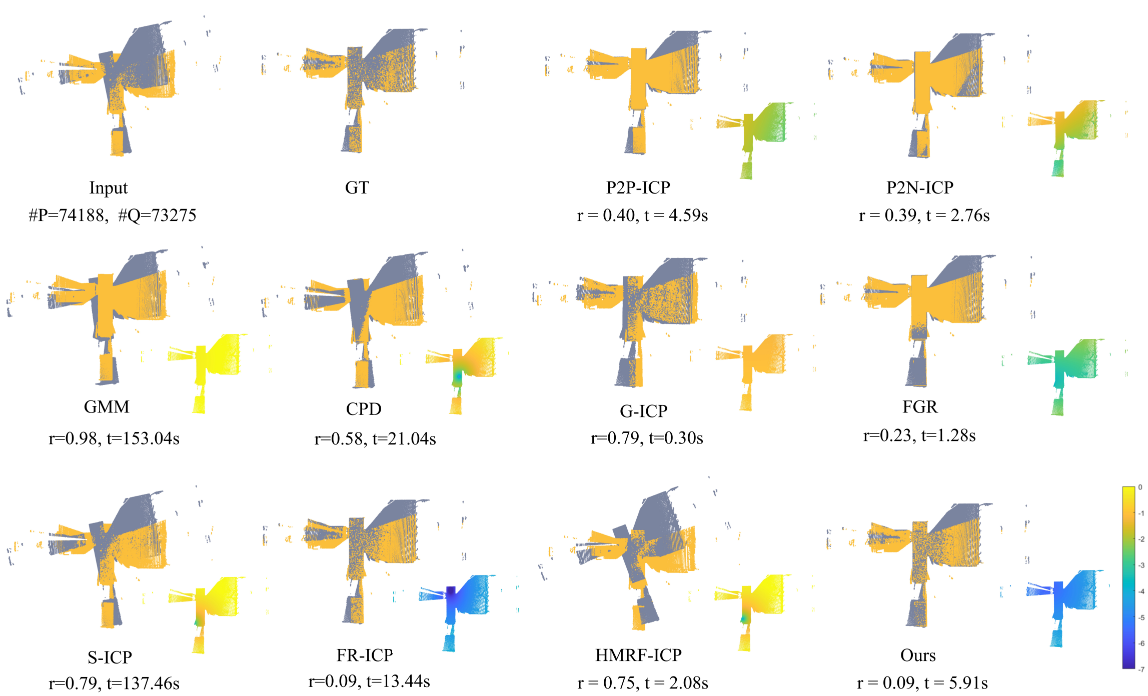

Figure 12. Registration results of different methods on ETH dataset. Our method and FR-ICP have the best performance, whereas our method consumes twofold less runtime as FR-ICP.

and FR-ICP enable high registration accuracy, meanwhile ours is faster than FR-ICP, the others lead to relatively large deviations.

For the KITTI dataset, we align the point clouds in the sequence whose index intervals are 1, 4 and 8. Larger index interval indicates lower overlapping rate. The experimental results with interval equal to 8 are reported in Fig. 13, of which circles indicate the zoom-in registration. As ob-

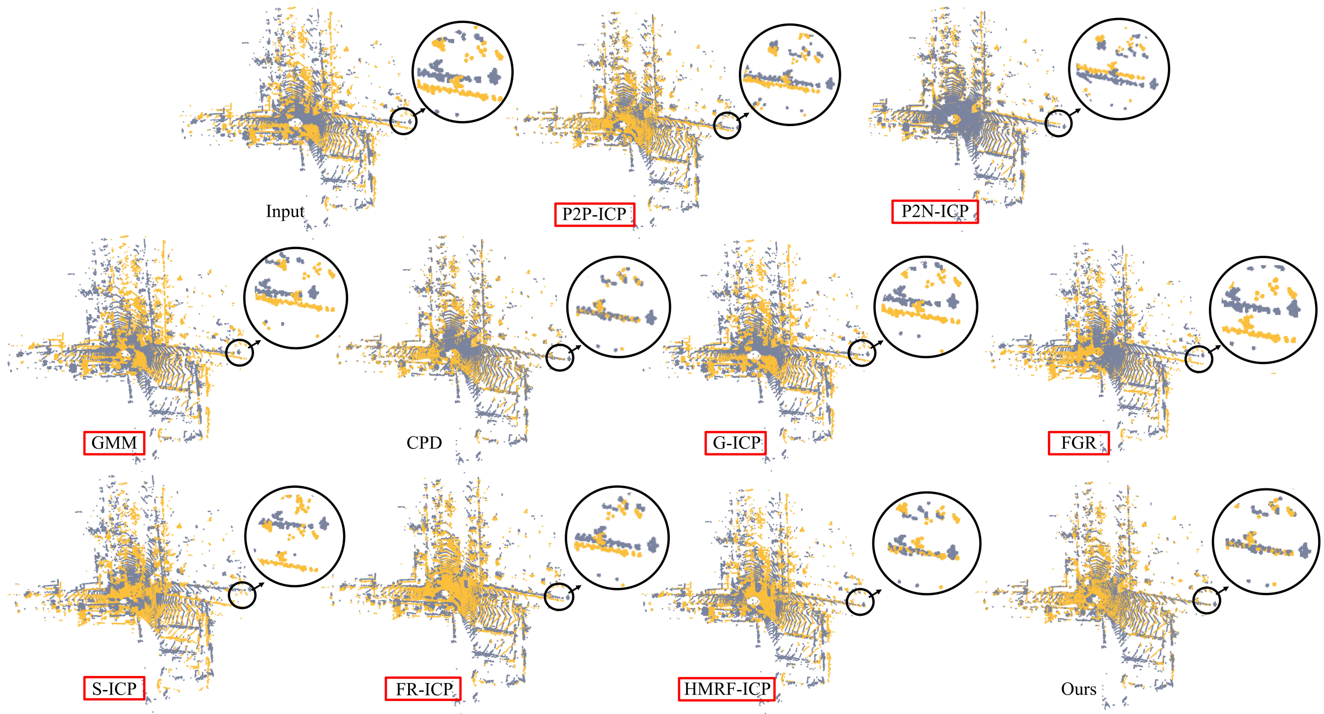

Figure 13. Registration results of the KITTI dataset with the index interval equal to 8. Red boxes indicate methods that have relatively large deviations and circles are the zoom-in results.

served, with the decrease of overlapping part between two point clouds, most methods produce significant registration error. However, our proposed algorithm still achieves accurate results. More registration results are reported in *Supplemental Material*.

5. Conclusions and Future Research

We presented a novel and robust method for accurate registration of low overlapping point clouds. We integrate geometric features with the probabilistic model hidden Markov random field to effectively infer overlapping regions between two point clouds and depress outlier contamination. We prove a necessary and sufficient condition when the preliminary symmetric function equals to zero, analyze its shortcomings, and introduce a curvature-aware symmetric function, which enables the pairwise point correspondence more discriminative, thereby ensuring more accurate registration. Additionally, we adopt linear approximation to the proposed objective function and then involve it into the geometrically stable sampling framework to achieve more stable transformations.

We assess the proposed method and compare it with representative state-of-the-art approaches on noisy, outlier-contaminated, different initialization, and low-overlapping settings, where results demonstrate that the proposed method outperforms competitors with higher accuracy and robustness along with reasonable time consumption, especially on low overlapping scenarios.

The currently proposed registration framework is limited to pairwise low overlapping point clouds, in the future, we plan to generalize it to multi-view low overlapping cases. For such challenging assignment, to avoid error accumulation between multiple transformations, we can theoretically formalize the task as a clustering problem and then explore solutions by probabilistic graph models.

Acknowledgement

The work is supported by National Key R&D Program of China (2021YFB1715900), and the National Natural Science of Foundation of China for Outstanding Young Scholars (12022117).

References

[1] Aim@shape Shape Repository. [Online]. Available. http://visionair.ge.imati.cnr.it/ontologies/shapes/. 11

[2] The Kitti Vision Benchmark Suite. [Online]. Available. http://www.cvlibs.net/datasets/kitti/. 6

[3] The Stanford 3D Scanning Repository. [Online]. Available. http://graphics.stanford.edu/data/3Dscanrep/. 6

[4] Terrestrial Laser Scanner Point Clouds. [Online]. Available. https://prs.igp.ethz.ch/research/completed_projects.html. 11

[5] Y. Aoki, H. Goforth, R. A. Srivatsan, and S. Lucey. Pointnetlk: Robust & efficient point cloud registration using pointnet. In *Proceedings of the IEEE/CVF Conference on Com-*

puter Vision and Pattern Recognition, pages 7163–7172, 2019. 3

[6] P. J. Besl and N. D. McKay. Method for registration of 3-d shapes. In *Sensor fusion IV: control paradigms and data structures*, volume 1611, pages 586–606. International Society for Optics and Photonics, 1992. 1, 2, 6, 7

[7] S. Bouaziz, A. Tagliasacchi, H. Li, and M. Pauly. Modern techniques and applications for real-time non-rigid registration. In *SIGGRAPH ASIA 2016 Courses*, pages 1–25. 2016. 2

[8] S. Bouaziz, A. Tagliasacchi, and M. Pauly. Sparse iterative closest point. In *Computer graphics forum*, volume 32, pages 113–123. Wiley Online Library, 2013. 2, 6

[9] S. P. Chatzis and T. A. Varvarigou. A fuzzy clustering approach toward hidden markov random field models for enhanced spatially constrained image segmentation. *IEEE Transactions on Fuzzy Systems*, 16(5):1351–1361, 2008. 2

[10] Y. Chen and G. Medioni. Object modelling by registration of multiple range images. *Image and Vision Computing*, 10(3):145–155, 1992. 2, 6, 7

[11] S. Choi, Q.-Y. Zhou, and V. Koltun. Robust reconstruction of indoor scenes. In *Proceedings of the IEEE Conference on Computer Vision and Pattern Recognition*, pages 5556–5565, 2015. 1

[12] C. Choy, W. Dong, and V. Koltun. Deep global registration. In *Proceedings of the IEEE/CVF conference on computer vision and pattern recognition*, pages 2514–2523, 2020. 3

[13] P. Clifford. Markov random fields in statistics. *Disorder in physical systems: A volume in honour of John M. Hammersley*, pages 19–32, 1990. 4

[14] M. Danelljan, G. Meneghetti, F. S. Khan, and M. Felsberg. A probabilistic framework for color-based point set registration. In *Proceedings of the IEEE Conference on Computer Vision and Pattern Recognition*, pages 1818–1826, 2016. 3

[15] B. Fang, G. Mei, X. Yuan, L. Wang, Z. Wang, and J. Wang. Visual slam for robot navigation in healthcare facility. *Pattern Recognition*, 113:107822, 2021. 1

[16] M. Fiorucci, M. Khoroshiltseva, M. Pontil, A. Traviglia, A. Del Bue, and S. James. Machine learning for cultural heritage: A survey. *Pattern Recognition Letters*, 133:102–108, 2020. 1

[17] A. Fusiello, U. Castellani, L. Ronchetti, and V. Murino. Model acquisition by registration of multiple acoustic range views. In *European Conference on Computer Vision*, pages 805–819, 2002. 3

[18] N. Gelfand, L. Ikemoto, S. Rusinkiewicz, and M. Levoy. Geometrically stable sampling for the icp algorithm. In *Fourth International Conference on 3-D Digital Imaging and Modeling, 2003. 3DIM 2003. Proceedings.*, pages 260–267. IEEE, 2003. 6

[19] O. Hirose. A bayesian formulation of coherent point drift. *IEEE Transactions on Pattern Analysis and Machine Intelligence*, 2020. 3

[20] H. Hontani, T. Matsuno, and Y. Sawada. Robust nonrigid icp using outlier-sparsity regularization. In *2012 IEEE Conference on Computer Vision and Pattern Recognition*, pages 174–181, 2012. 2

[21] B. Jian and B. C. Vemuri. Robust point set registration using gaussian mixture models. *IEEE Transactions on Pattern Analysis and Machine Intelligence*, 33(8):1633–1645, 2010. 3, 6, 7

[22] R. Kolluri, J. R. Shewchuk, and J. F. O'Brien. Spectral surface reconstruction from noisy point clouds. In *Proceedings of the 2004 Eurographics/ACM SIGGRAPH symposium on Geometry processing*, pages 11–21, 2004. 6

[23] F. J. Lawin, M. Danelljan, F. S. Khan, P.-E. Forssén, and M. Felsberg. Density adaptive point set registration. In *Proceedings of the IEEE Conference on Computer Vision and Pattern Recognition*, pages 3829–3837, 2018. 3

[24] W. Lu, G. Wan, Y. Zhou, X. Fu, P. Yuan, and S. Song. Deepvcp: An end-to-end deep neural network for point cloud registration. In *Proceedings of the IEEE/CVF International Conference on Computer Vision*, pages 12–21, 2019. 3

[25] B. D. Lucas, T. Kanade, et al. An iterative image registration technique with an application to stereo vision. 1981. 3

[26] R. Muñoz-Salinas and R. Medina-Carnicer. Ucoslam: Simultaneous localization and mapping by fusion of keypoints and squared planar markers. *Pattern Recognition*, 101:107193, 2020. 1

[27] A. Myronenko and X. Song. Point set registration: Coherent point drift. *IEEE Transactions on Pattern Analysis and Machine Intelligence*, 32(12):2262–2275, 2010. 3, 6, 7

[28] H. Pottmann, Q.-X. Huang, Y.-L. Yang, and S.-M. Hu. Geometry and convergence analysis of algorithms for registration of 3d shapes. *International Journal of Computer Vision*, 67(3):277–296, 2006. 2

[29] C. R. Qi, H. Su, K. Mo, and L. J. Guibas. Pointnet: Deep learning on point sets for 3d classification and segmentation. In *Proceedings of the IEEE conference on computer vision and pattern recognition*, pages 652–660, 2017. 3

[30] S. Rusinkiewicz. A symmetric objective function for icp. *ACM Transactions on Graphics (TOG)*, 38(4):1–7, 2019. 2, 4, 5

[31] A. Segal, D. Haehnel, and S. Thrun. Generalized-icp. In *Robotics: science and systems*, volume 2, page 435. Seattle, WA, 2009. 6

[32] J. Stechschulte, N. Ahmed, and C. Heckman. Robust low-overlap 3-d point cloud registration for outlier rejection. In *2019 International Conference on Robotics and Automation (ICRA)*, pages 7143–7149, 2019. 2, 3, 4, 5, 6, 7

[33] J. Sturm, N. Engelhard, F. Endres, W. Burgard, and D. Cremers. A benchmark for the evaluation of rgb-d slam systems. In *2012 IEEE/RSJ international conference on intelligent robots and systems*, pages 573–580, 2012. 8

[34] W. Tabib, C. O'Meadhra, and N. Michael. On-manifold gmm registration. *IEEE Robotics and Automation Letters*, 3(4):3805–3812, 2018. 3

[35] G. K. Tam, Z.-Q. Cheng, Y.-K. Lai, F. C. Langbein, Y. Liu, D. Marshall, R. R. Martin, X.-F. Sun, and P. L. Rosin. Registration of 3d point clouds and meshes: A survey from rigid to nonrigid. *IEEE Transactions on Visualization and Computer Graphics*, 19(7):1199–1217, 2012. 2

[36] C. Thomson, G. Apostolopoulos, D. Backes, and J. Boehm. Mobile laser scanning for indoor modelling. *ISPRS Ann.*

Photogramm. Remote Sens. Spat. Inf. Sci, 5(W2):66, 2013. 1

[37] S. Umeyama. Least-squares estimation of transformation parameters between two point patterns. *IEEE Transactions on Pattern Analysis and Machine Intelligence*, 13(04):376–380, 1991. 1

[38] W. Wang, H. Pottmann, and Y. Liu. Fitting B-spline curves to point clouds by curvature-based squared distance minimization. *ACM Transactions on Graphics (TOG)*, 25(2):214–238, 2006. 2

[39] Y. Wang and J. M. Solomon. Deep closest point: Learning representations for point cloud registration. In *Proceedings of the IEEE/CVF International Conference on Computer Vision*, pages 3523–3532, 2019. 3

[40] J. Zhang, Y. Yao, and B. Deng. Fast and robust iterative closest point. *IEEE Transactions on Pattern Analysis and Machine Intelligence*, 2021. 2, 6

[41] Q.-Y. Zhou, J. Park, and V. Koltun. Fast global registration. In *European conference on computer vision*, pages 766–782, 2016. 2, 6